2023 IEEE International Conference on Robotics and Automation (ICRA 2023)
May 29 - June 2, 2023. London, UK

Bidirectional Generalised Rigid Point Set Registration

Ang Zhang†, Zhe Min†, Li Liu, Max Q.-H. Meng, *Fellow, IEEE*

***Abstract*— In medical robotics and image-guided surgery (IGS), registration is needed in order to align together the coordinate frames of robots, medical imaging modalities, surgical tools, and patients. Existing registration algorithms often assume one point set to be a noise-free model while the other to contain noise and outliers. However, in real scenarios, noise and outliers can exist in both point sets to be registered. To eliminate the above-mentioned challenge, in this paper, we formally formulate the Bi-directional Generalised Rigid Point Set Registration (Bi-GRPSR) problem where normal vectors are adopted, bi-directional probability density function (PDFs) and Hybrid Mixture Models (HMMs) are constructed to derive the objective function. Bi-GRPSR considering anisotropic positional noise is thus cast as a maximum likelihood estimation (MLE) problem, which is solved by the proposed Bi-directional Generalised Anisotropic Coherent Point Drift (Bi-AGCPD) where spatially nearby points are considered to move coherently and iterative expectation maximization (EM) steps are involved. Experimental results on two human bone point sets, under different settings of noise, outliers, and overlapping ratios, validate the effectiveness and improvements of Bi-AGCPD over existing probabilistic and learning-based methods.**

I. Introduction

Registration is one key problem that affects the overall interventional accuracy for a medical robotic system and image-guided surgery (IGS) [1], [2]. As one typical application of registration in IGS, it brings together the pre-operative space where the surgical plan is tailored to the intra-operative space where the actual surgical operation is done. Registration aims to estimate the transformation parameters (e.g., rigid, affine, or non-rigid) that best align two spatial spaces, by optimizing certain similarity measures (e.g., intensity difference, cross correlation, Euclidean or Mahalanobis distance) over images or features (e.g., points, lines, planes, etc.) [3]–[7]. Registration algorithms are susceptible to noise and outliers, which makes it challenging to have a perfect solution for real-world applications [8]–[11].

Most of existing registration methods assume one point set to be noise-free while the other to contain noise/outliers [4], [12]–[15]. In IGS, however, both point sets extracted from the pre-operative volumetric medical images and intra-operative surgical tools respectively could be contaminated by noise/outliers [16]–[18]. For example, the pre-operative CT image usually has a spatial resolution of around ~ 0.5 mm in the x-y plane and $0.5 - 0.625$ mm in the z axis [19][20]. Intra-operatively, the magnitude of marker localisation error is ~ 0.25mm in a typical NDI optical tracking system [19][20].

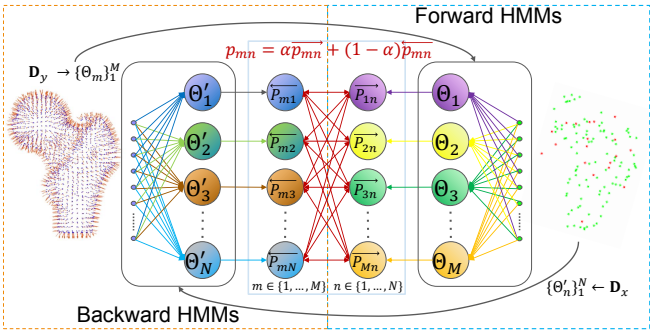

Fig. 1. Illustration of the Bidirectional Generalised Rigid Point Set Registration (BGRPSR) to estimate the rotation $\mathbf{R}$ and the translation $\mathbf{t}$. In the forward HMM, each generalised point $\mathbf{T}(\mathbf{d}_m^y) = [\mathbf{R}\mathbf{y}_m + \mathbf{t}; \mathbf{R}\widehat{\mathbf{y}}_m]$ is utilised to compose one component $\mathbf{\Theta}_m$ of the forward Hybrid Mixture Models (HMMs), from which $\mathbf{d}_n^x = [\mathbf{x}_n; \widehat{\mathbf{x}}_n]$ is generated and forward posteriors $\overrightarrow{p}_{mn}$ are computed for $n = 1, .., N$. In contrast, each $\mathbf{T}^{-1}(\mathbf{d}_n^x) = [\mathbf{R}^\intercal\mathbf{x}_n - \mathbf{R}^\intercal\mathbf{t}; \mathbf{R}^\intercal\widehat{\mathbf{x}}_n]$ composes one component $\mathbf{\Theta}'_n$ of backward HMMs, from which $\mathbf{d}_m^y$ is randomly generated and backward posteriors $\overleftarrow{p}_{mn}$ are computed for $m = 1, ...M$. The posterior p_{mn} is the weighted value of the $\overrightarrow{p}_{mn}$ and $\overleftarrow{p}_{mn}$. In the middle, we only show the process of generating weighted posterior from $\overrightarrow{p}_{in} (i \in \{1, ..., M\})$ and $\overrightarrow{p}_{mj} (j \in \{1, ..., N\})$ for specific n and m, which will indeed be repeated for all $n \in \{1, ..., N\}$ and $m \in \{1, ..., M\}$.

Motivations As we have introduced, in real-world applications, both points could contain noise/outliers. To ease this issue, the idea is to first consider point sets $\mathbf{X}$ and $\mathbf{Y}$ to be model and data point sets respectively, and then reversely consider point sets $\mathbf{X}$ and $\mathbf{Y}$ to be data and model point sets respectively. Computing the posterior probabilities in a bidirectional way has great potential to reduce the confidence bias towards one specific point set. At the same time, the additional features (e.g., normal vectors) extracted from the raw point set have great potential of not only helping distinguish outliers from inliers and thus enhancing the registration robustness, but also providing more information and improving accuracy. In addition, the positional noise is assumed to be anisotropic, e.g., the standard deviation of marker localisation error in the viewing direction is 3-5 times of those in the other two directions [19], [20].

Contributions In this paper, we formally define the Bidirec-

†Equal contribution.

Ang Zhang and Li Liu are with the Department of Electronic Engineering, The Chinese University of Hong Kong, N.T., Hong Kong SAR, China.

Zhe Min is with the School of Control Science and Engineering, Shandong University, China, and also with Wellcome/EPSRC Centre for Surgical and Interventional Sciences, University College London, UK.

Max Q.-H. Meng is with the Department of Electronic and Electrical Engineering of the Southern University of Science and Technology, Shenzhen, China, on leave from the Department of Electronic Engineering, The Chinese University of Hong Kong, Hong Kong, and also with the Shenzhen Research Institute of the Chinese University of Hong Kong, Shenzhen, China max.meng@ieee.org.

This project is partially supported by National Key R&D program of China with Grant No. 2019YFB1312400 and Hong Kong RGC GRF grants #14211420 awarded to Max Q.-H. Meng. *(Corresponding author: Li Liu, Max Q.-H. Meng.)*

tional Generalised Rigid Point Set Registration (BGRPSR) problem and its iterative expectation maximisation solution Bi-directional Generalised Anisotropic Coherent Point Drift (Bi-AGCPD), under both isotropic and anisotropic positional uncertainties. Our contributions can be summarised as follows. First, the probability density function (PDF) of the 'data' points is constructed in a bidirectional way, with Gaussian and Fisher distributions being used for modeling localisation uncertainties with positional and normal vectors respectively. The hybrid mixture models (HMMs) are then formulated accordingly, with which the objective function of the maximum likelihood estimation (MLE) problem is derived. Second, expectation maximisation (EM) technique is utilised to solve the above MLE problem under both isotropic and anisotropic uncertainties. Third, Bi-AGCPD is validated against both conventional and deep-learning-based methods on various human bone models under different settings of noise, outliers, and overlapping ratios.

Organisations This paper is organised as follows. Section. II introduces the related point set registration methods. Section. III introduces the forward/backward PDFs and HMMs. Section. IV formally defines the BGRPSR problem and presents the iterative Bi-AGCPD algorithm. Section. V presents the experiments and results. Section. VI concludes the paper.

II. Related Work

There are a large amount of point set registration methods in the literature [3][4][21]. Here, we review the most related rigid registration approaches in three categories: ICP-based methods, probabilistic methods, deep-learning-based, and feature-based registration methods.

ICP-based Methods The correspondences between points in two point sets to be registered are usually not known. The classical Iterative Closest Point (ICP) method tackles the registration as follows: the closest point in one point set is found for each point in the other point set based on the Euclidean distance; the rotation and translation are estimated with the point correspondences and singular value decomposition (SVD) technique [22]. The assumptions in the ICP include: a) one point set is considered as the noise-free model; b) the positional noise is assumed to be isotropic (i.e., the same in the three directions); c) the noise vectors are also assumed to be independent and identically distributed (i.i.d.) [22]. Go-ICP intends to guarantee a global registration solution with the Branch-and-Bound technique [23]. There also exist other ICP-based methods [24], [25]

Probabilistic Methods To enhance the registration algorithm's robustness to noise/outliers, various noise models have been used to formulate the point set registration problem [26]. Gaussian Mixture Model (GMM)-based registration method assumes one point set to be GMMs' centers and the other to be the data point set, points in which are generated randomly from the transformed model point set [12], [13], [27], [28]. In the Coherent Point Drift (CPD) method, the alignment of two point sets is cast as a probability density estimation problem and the negative log-likelihood function is minimised to estimate the transformation parameters [12]. GMMReg regards both point sets as the centroids of two respective GMMs, the L2 distance of which is minimised to register the two point sets [27]. Very recently, BCPD reformulates both the rigid and non-rigid registration problems into the Bayesian framework, where the algorithms' theoretical convergence is guaranteed [13].

Deep-learning-based Methods The learning-based methods either first learn robust features with deep neural networks to estimate correct correspondence and then transformation is estimated using one-step optimisation (SVD or RANSAC) [29], [30], or estimate the transformation with an end-to-end neural network [31]–[36]. Among others, DeepGMR is the learning-based registration that explicitly leverages the probabilistic paradigm, where point-to-GMMs correspondences are learnt through a neural network and transformation/GMMs parameters are estimated by a forward step [34].

Feature-based Registration Methods The additional features (e.g., tangent or normal vectors) extracted from raw point sets (e.g., curves, surfaces) can facilitate and enhance the registration process [37]–[41]. In IGBCPD, the normal-assisted generalised rigid point set registration is reformulated into the BCPD framework to certify the theoretical convergence [14]. AGBCPD further generalises the positional error distributions in IGBCPD from isotropic to anisotropic [15].

III. Bidirectional Probability Density Function (PDF) and Hybrid Mixture Models (HMMs)

In Generalised Rigid Point Set Registration (GRPSR), the rigid transformation including rotation $\mathbf{R} \in SO(3)$ and translation $\mathbf{t} \in \mathbb{R}^3$ between two spaces is estimated given $\mathbf{x}_n \in \mathbb{R}^3, \widehat{\mathbf{x}}_n(||\mathbf{x}_n|| = 1) \in \mathbb{R}^3$ and $\mathbf{y}_m \in \mathbb{R}^3, \widehat{\mathbf{y}}_m(||\mathbf{y}_m|| = 1) \in \mathbb{R}^3$ (positional and unit normal vectors). The idea is to consider the point set registration in a bidirectional manner, i.e., forward and backward ways. In the forward way, $\mathbf{d}_n^x = [\mathbf{x}_n; \widehat{\mathbf{x}}_n]$ are considered as generalised data points sampled from Hybrid Mixture Models (HMMs) composed of Gaussian Mixture Model (GMM) and Fisher Mixture Model (FMM) centering at transformed generalised model points $[\mathbf{R}\mathbf{y}_m + \mathbf{t}; \mathbf{R}\widehat{\mathbf{y}}_m]$ with additional noise. In the backward way, $\mathbf{d}_m^y = [\mathbf{y}_m; \widehat{\mathbf{y}}_m]$ are considered as data points sampled from HMMs centering at transformed model points $[\mathbf{R}^\mathsf{T}\mathbf{x}_n - \mathbf{R}^\mathsf{T}\mathbf{t}; \mathbf{R}^\mathsf{T}\widehat{\mathbf{x}}_n]$. The proposed bi-directional mechanism is illustrated in Fig. 1.

Forward PDF In the case of anisotropic positional uncertainty, the forward probability density function (PDF) of the n-th point $\mathbf{d}_n^x$ in $\mathbf{X}$ is defined as

$$
\begin{aligned}
&p\left(\mathbf{d}_n^x \mid \overrightarrow{c}_n = m; \mathbf{\Theta}\right) = \\
&\underbrace{\frac{\kappa}{2\pi\left(e^{\kappa} - e^{-\kappa}\right)} e^{\kappa(\mathbf{R}\widehat{\mathbf{y}}_m)^\top \widehat{\mathbf{x}}_n}}_{\widehat{\mathbf{x}}_n \sim \mathcal{F}(\mathbf{R}\widehat{\mathbf{y}}_m, \kappa)} \cdot \underbrace{\frac{1}{\sqrt{(2\pi)^3 |\mathbf{\Sigma}|}} e^{-\frac{1}{2}\overrightarrow{\mathbf{z}}_{mn}^\mathsf{T} \mathbf{\Sigma}^{-1} \overrightarrow{\mathbf{z}}_{mn}}}_{\mathbf{x}_n \sim \mathcal{N}(\mathbf{R}\mathbf{y}_m + \mathbf{t}, \mathbf{\Sigma})} \\
&= \frac{\kappa}{(2\pi)^{\frac{5}{2}} |\mathbf{\Sigma}| \cdot \left(e^{\kappa} - e^{-\kappa}\right)} e^{\kappa(\mathbf{R}\widehat{\mathbf{y}}_m)^\top \widehat{\mathbf{x}}_n - \frac{1}{2}\overrightarrow{\mathbf{z}}_{mn}^\mathsf{T} \mathbf{\Sigma}^{-1} \overrightarrow{\mathbf{z}}_{mn}},
\end{aligned}
\tag{1}
$$

where $\overrightarrow{c}_n \in \{1,2,3,...,M\}$ is the forward latent variable that indicates the point correspondences for $n \in \{1,2,3,...,N\}$, $\mathbf{\Theta} = \{\mathbf{R}, \mathbf{t}, \kappa, \mathbf{\Sigma}\}$, $\mathbf{\Sigma} \in \mathbb{S}^3$ is the anisotropic positional covariance, $|\mathbf{\Sigma}|$ is the determinant of $\mathbf{\Sigma}$, $\kappa \in \mathbb{R}$ is the concentration parameter with the normal vector, $\overrightarrow{\mathbf{z}}_{mn} = \mathbf{x}_n - (\mathbf{R}\mathbf{y}_m + \mathbf{t})$ is the distance vector between the point $\mathbf{x}_n$ and rigidly transformed point $(\mathbf{R}\mathbf{y}_m + \mathbf{t})$, we can see from the above the forward PDF is the product of the Fisher distribution whose centroid is $\mathbf{R}\widehat{\mathbf{y}}_m$ and multi-variate Gaussian distribution whose center is $\mathbf{R}\mathbf{y}_m + \mathbf{t}$.

Backward PDF Similarly, the backward PDF of the m-th point $\mathbf{d}_m^y$ in $\mathbf{Y}$ is defined as

$$\begin{aligned} &p\left(\mathbf{d}_m^y \mid \overleftarrow{c}_m = n; \mathbf{\Theta}\right) = \\ &\underbrace{\frac{\kappa}{2\pi\left(e^{\kappa} - e^{-\kappa}\right)} e^{\kappa\left(\mathbf{R}^{\mathsf{T}}\widehat{\mathbf{x}}_n\right)^{\mathsf{T}}\widehat{\mathbf{y}}_m}}_{\widehat{\mathbf{y}}_m \sim \mathcal{F}\left(\mathbf{R}^{\mathsf{T}}\widehat{\mathbf{x}}_n, \kappa\right)} \cdot \underbrace{\frac{1}{\sqrt{(2\pi)^3 |\mathbf{\Sigma}|}} e^{-\frac{1}{2}\overleftarrow{\mathbf{z}}_{mn}^{\mathsf{T}}\mathbf{\Sigma}^{-1}\overleftarrow{\mathbf{z}}_{mn}}}_{\mathbf{y}_m \sim \mathcal{N}\left(\mathbf{R}^{\mathsf{T}}\mathbf{x}_n - \mathbf{R}^{\mathsf{T}}\mathbf{t}, \mathbf{\Sigma}\right)} \\ &= \frac{\kappa}{(2\pi)^{\frac{5}{2}} |\mathbf{\Sigma}| \cdot \left(e^{\kappa} - e^{-\kappa}\right)} e^{\kappa\left(\mathbf{R}^{\mathsf{T}}\widehat{\mathbf{x}}_n\right)^{\mathsf{T}}\widehat{\mathbf{y}}_m - \frac{1}{2}\overleftarrow{\mathbf{z}}_{mn}^{\mathsf{T}}\mathbf{\Sigma}^{-1}\overleftarrow{\mathbf{z}}_{mn}}, \end{aligned} \tag{2}$$

where $\overleftarrow{c}_m \in \{1,2,3,...,N\}$ is the backward latent variable that indicates the point correspondences for $m \in \{1,2,3,...,M\}$, $\overleftarrow{\mathbf{z}}_{mn} = \mathbf{y}_m - \left(\mathbf{R}^{\mathsf{T}}\mathbf{x}_n - \mathbf{R}^{\mathsf{T}}\mathbf{t}\right)$ is the distance vector between the point $\mathbf{y}_m$ and the rigidly transformed point $\left(\mathbf{R}^{\mathsf{T}}\mathbf{x}_n - \mathbf{R}^{\mathsf{T}}\mathbf{t}\right)$, the backward PDF is the product of the Fisher distribution whose centroid is $\mathbf{R}^{\mathsf{T}}\mathbf{x}_n$ and the multi-variate Gaussian distribution whose center is $\left(\mathbf{R}^{\mathsf{T}}\mathbf{x}_n - \mathbf{R}^{\mathsf{T}}\mathbf{t}\right)$. It is noted that the inherent meanings of $\overrightarrow{c}_n = m$ and $\overleftarrow{c}_m = n$ are the same, which both implicitly means that $\mathbf{d}_n^x$ corresponds with $\mathbf{d}_m^y$.

Forward HMMs The forward hybrid mixture models (HMMs) are respectively as follows

$$p(\mathbf{d}_n^x) = w\frac{1}{N} + (1-w)\sum_{m=1}^{M}\frac{1}{M}p(\mathbf{d}_n^x|\overrightarrow{c}_n = m; \mathbf{\Theta}) \tag{3}$$

where $w \in \mathbb{R}$ is the weight with the outlier distribution $p(\mathbf{d}_n^x|\overrightarrow{c}_n = M+1)$, and the inlier distribution $p(\mathbf{d}_n^x|\overrightarrow{c}_n = m; \mathbf{\Theta})$ is defined in (1). The inherent meaning is that the point $\mathbf{d}_n^x$ can either be generated from the transformed generalised points $\mathbf{d}_m^y$ with $\mathbf{R}$ and $\mathbf{t}$ or as an outlier.

Backward HMMs Correspondingly, the backward HMMs is defined as

$$p(\mathbf{d}_m^y) = w\frac{1}{M} + (1-w)\sum_{n=1}^{N}\frac{1}{N}p(\mathbf{d}_m^y|\overleftarrow{c}_m = n; \mathbf{\Theta}) \tag{4}$$

where the outlier distribution is defined as $p(\mathbf{d}_m^y|\overleftarrow{c}_m = N+1) = \frac{1}{M}$, and the inlier distribution $p(\mathbf{d}_m^y|\overleftarrow{c}_m = n; \mathbf{\Theta})$ is defined in (2). The inherent meaning of the formula is that the point $\mathbf{d}_m^y$ can either be generated from the transformed points $\mathbf{d}_n^x$ or is considered as an outlier.

IV. Bidirectional Generalised Rigid Point Set Registration (BGRPSR)

Objective Function Given the bi-directional HMMs defined in (3) and (4), the negative log-likelihood function to be minimised over $\mathbf{\Theta}$ is $E(\mathbf{\Theta}) = -\left(\sum_{n=1}^{N}\log p(\mathbf{d}_n^x) + \sum_{m=1}^{M}\log p(\mathbf{d}_m^y)\right)$, where we have utilised the i.i.d. assumption following CPD [12]. The rigid point set registration is formulated as a maximum likelihood estimation (MLE) problem, whose objective function is the expectation of the complete negative log-likelihood function $E(\mathbf{\Theta})$ as follows,

$$\begin{aligned} \mathcal{L}(\mathbf{\Theta}) = &-\frac{1}{2}N_{\mathbf{P}}\log|\mathbf{\Sigma}| - N_{\mathbf{P}}\log\left(e^{\kappa} - e^{-\kappa}\right) + N_{\mathbf{P}}\log\kappa \\ &- \sum_{n=1}^{N}\sum_{m=1}^{M} p_{mn}\left(\frac{1}{2}\overrightarrow{\mathbf{z}}_{mn}^{\mathsf{T}}\mathbf{\Sigma}^{-1}\overrightarrow{\mathbf{z}}_{mn} - \kappa\left(\left(\mathbf{R}\widehat{\mathbf{y}}_m\right)^{\mathsf{T}}\widehat{\mathbf{x}}_n\right)\right) \end{aligned} \tag{5}$$

where p_{mn} is the bi-directional posterior probability that considers both the forward and backward HMMs, $N_{\mathbf{P}} = \sum_{n=1}^{N}\sum_{m=1}^{M} p_{mn}$ is the sum of bi-directional posteriors. We will show how the bi-directional posteriors are computed. It is noteworthy that the derivation of $\mathcal{L}(\mathbf{\Theta})$ in (5) is attributed to the fact that $\overrightarrow{\mathbf{z}}_{mn}^{\mathsf{T}}\mathbf{\Sigma}^{-1}\overrightarrow{\mathbf{z}}_{mn}$ is equal to $\overleftarrow{\mathbf{z}}_{mn}^{\mathsf{T}}\mathbf{\Sigma}^{-1}\overleftarrow{\mathbf{z}}_{mn}$, which is the Mahalanobis distance between the two points. The expectation maximisation (EM) steps are utilised to solve the MLE problem.

Expectation Step In the expectation step, the probabilities that one point in $\mathbf{X}$ corresponds to one point in $\mathbf{Y}$ are computed. The forward posterior probability of $\mathbf{d}_m^y$ corresponding to $\mathbf{d}_n^x$ is

$$p(c_n = m|\mathbf{d}_n^x) = \frac{(1-w)\frac{1}{M}ab}{(1-w)\sum_{m=1}^{M}\frac{1}{m}ab + w\frac{1}{N}}, \tag{6}$$

and the backward posterior probability is defined as

$$p(c_n = m|\mathbf{d}_m^y) = \frac{(1-w)\frac{1}{N}ab}{(1-w)\sum_{n=1}^{N}\frac{1}{N}ab + w\frac{1}{M}} \tag{7}$$

where the full expressions of shorthand a and b are as follows

$$\begin{aligned} a &= \frac{\kappa}{(2\pi)^{\frac{5}{2}}|\mathbf{\Sigma}| \cdot \left(e^{\kappa} - e^{-\kappa}\right)} \\ b &= \kappa\left(\mathbf{R}^{\mathsf{T}}\widehat{\mathbf{x}}_n\right)^{\mathsf{T}}\widehat{\mathbf{y}}_m - \frac{1}{2}\overrightarrow{\mathbf{z}}_{mn}^{\mathsf{T}}\mathbf{\Sigma}^{-1}\overrightarrow{\mathbf{z}}_{mn} \end{aligned} \tag{8}$$

For simplicity, we utilise the following shorthands,

$$\begin{aligned} \overrightarrow{p}_{mn} &= p(c_n = m|\mathbf{d}_n^x) \\ \overleftarrow{p}_{mn} &= p(c_n = m|\mathbf{d}_m^y) \end{aligned} \tag{9}$$

The utilised bi-directional posterior probability is the weighted average of the forward and backward posteriors as:

$$p_{mn} = \alpha\overrightarrow{p}_{mn} + (1-\alpha)\overleftarrow{p}_{mn} \tag{10}$$

where $\alpha \in \mathbb{R}^3$ (the default value is 0.5) is the weight with the forward posterior probability.

Maximization Rigid Transformation Step Referring to (5), the objective function that is related to the rotation matrix and translation vector is simplified to

$$\mathcal{L}(\mathbf{R}, \mathbf{t}) = \sum_{n,m=1}^{N,M} p_{mn}\left(\kappa\left(\left(\mathbf{R}\widehat{\mathbf{y}}_m\right)^{\mathsf{T}}\widehat{\mathbf{x}}_n\right) - \frac{1}{2}\overrightarrow{\mathbf{z}}_{mn}^{\mathsf{T}}\mathbf{\Sigma}^{-1}\overrightarrow{\mathbf{z}}_{mn}\right) \tag{11}$$

The Rodrigues' rotation formula is utilised to represent $\mathbf{R}$ with a vector $\boldsymbol{\theta} \in \mathbb{R}^3$. Then we construct $\boldsymbol{\varphi} = [\boldsymbol{\theta}; \mathbf{t}] \in \mathbb{R}^6$,

TABLE I
ROTATION AND TRANSLATION ERRORS UNDER ISOTROPIC/ANISOTROPIC NOISE TOGETHER WITH DIFFERENT PERCENTAGES OF OUTLIERS IN $\mathbf{D}_x$. FULL-TO-FULL REGISTRATION OF HUMAN FEMUR BONE.

Error Type	Outliers' Percents	10%	30%	50%	70%	90%	10%	30%	50%	70%	90%
	Noise type / Methods	Isotropic Noise					Anisotropic Noise				
Rot (°)	ICP [22]	2.6877	3.9594	4.8543	5.3575	5.2281	2.0556	3.1001	4.5424	4.6535	4.6680
	CPD [12]	1.8358	2.6128	3.0104	4.4782	4.7743	0.4017	0.3893	0.3709	0.4337	0.4050
	BCPD [13]	2.2952	2.5879	2.6730	3.1432	3.0453	1.8640	1.6205	2.8059	3.2267	3.5296
	DeepGMR [34]	46.317	50.399	40.267	41.946	42.033	37.855	50.005	44.908	43.889	37.498
	IGBCPD [14]	0.9530	1.0353	1.1096	0.9228	1.1005	0.3624	0.3586	0.4056	0.3391	0.4437
	AGBCPD [15]	0.9523	0.8310	1.0660	0.9795	0.9304	0.2759	0.3204	0.3670	0.3093	0.2792
	Bi-IGCPD	0.4551	0.5047	0.5486	0.5444	0.5256	0.1396	0.1300	0.1510	0.1429	0.1785
	Bi-AGCPD	**0.4456**	**0.4743**	**0.4976**	**0.5148**	**0.4999**	**0.1184**	**0.1240**	**0.1273**	**0.1150**	**0.1410**
Trans (mm)	ICP [22]	1.0479	1.6958	1.8395	2.1533	2.0304	0.9169	1.4334	1.8280	1.9296	1.7418
	CPD [12]	0.7763	1.0165	0.8221	1.8000	1.8764	0.2940	0.2792	0.2801	0.2907	0.2649
	BCPD [13]	1.2921	1.5420	1.5816	1.7923	2.0431	0.6056	0.9009	0.9917	1.3338	1.3467
	DeepGMR [34]	16.295	15.161	15.770	15.490	14.996	16.137	15.727	15.239	15.073	15.419
	IGBCPD [14]	0.4804	0.5228	0.5204	0.5633	0.4781	0.3008	0.2624	0.3060	0.2837	0.3241
	AGBCPD [15]	0.4526	0.5171	0.5147	0.4974	0.4981	0.2521	0.2445	0.2021	0.2263	0.2119
	Bi-IGCPD	0.2667	0.2487	0.2500	0.2703	0.2680	0.1308	0.1233	0.1421	0.1524	0.1652
	Bi-AGCPD	**0.2358**	**0.2232**	**0.2155**	**0.2681**	**0.2428**	**0.1010**	**0.1004**	**0.1012**	**0.0982**	**0.1001**

and the above objective function $\mathcal{L}(\mathbf{R}, \mathbf{t})$ is reformulated into $\mathcal{L}(\boldsymbol{\varphi})$, whose value is estimated by solving $\frac{\partial \mathcal{L}(\boldsymbol{\varphi})}{\partial \boldsymbol{\varphi}} = \mathbf{0}$. The successive rotation/translation is computed by applying the Rodrigues' formula back. More details including formulas of the explicit gradients can be found in our recent work[15].

Maximization Covariance Step The objective function that is related to $\boldsymbol{\Sigma}$ is as follows,

$$\mathcal{L}(\boldsymbol{\Sigma}) = -\frac{1}{2} N_{\mathbf{P}} \log |\boldsymbol{\Sigma}| - \sum_{n=1}^{N} \sum_{m=1}^{M} p_{mn} \frac{1}{2} \overrightarrow{\mathbf{z}}_{mn}^{\mathsf{T}} \boldsymbol{\Sigma}^{-1} \overrightarrow{\mathbf{z}}_{mn} \tag{12}$$

By solving $\frac{\partial \mathcal{L}(\boldsymbol{\Sigma})}{\partial \boldsymbol{\Sigma}} = \mathbf{0}$, we can get the updated covariance matrix as

$$\boldsymbol{\Sigma} = \sum_{n,m=1}^{N,M} p_{mn} \overrightarrow{\mathbf{z}}_{mn} \overrightarrow{\mathbf{z}}_{mn}^{\mathsf{T}} / N_{\mathbf{p}}. \tag{13}$$

Maximization Concentration Parameter Step The objective function that is related to κ is as follows,

$$\begin{aligned} \mathcal{L}(\kappa) = & -N_{\mathbf{P}} \log \left(e^{\kappa} - e^{-\kappa}\right) + N_{\mathbf{P}} \log \kappa \\ & + \sum_{n,m=1}^{N,M} p_{mn} \kappa \left((\mathbf{R} \widehat{\mathbf{y}}_m)^{\mathsf{T}} \widehat{\mathbf{x}}_n \right) \end{aligned} \tag{14}$$

The derivative of $\mathcal{L}(\kappa)$ with respect to κ, i.e. $\frac{\partial \mathcal{L}(\kappa)}{\partial \kappa}$ is

$$-\frac{1}{\kappa} + \frac{e^{\kappa} + e^{-\kappa}}{e^{\kappa} - e^{-\kappa}} = \frac{1}{N_{\mathbf{P}}} \sum_{m=1}^{M} \sum_{n=1}^{N} p_{mn} \left(\mathbf{R}^i \widehat{\mathbf{y}}_m \right)^{\mathsf{T}} \widehat{\mathbf{x}}_n. \tag{15}$$

which is solved with the fixed-point iteration technique.

The above expectation and maximisation steps in (10), (11), (13) and (15) will be conducted iteratively until convergence. In Section III and Section IV, we present the probabilistic models, objective function and procedures under anisotropic positional noise. In the case of isotropic positional noise, the $\boldsymbol{\Sigma}$ is replaced with σ^2 in (1), (2), (8), (5) and the algorithm is denoted as Bi-directional Generalised Isotropic Coherent Point Drift (Bi-IGCPD). We omit the details which the readers are referred to our recent work [14].

V. EXPERIMENTAL RESULTS

Experiments have been done on the human femur and pelvis bone point sets, where the corresponding clinical application is to align together two spaces of pre-operative surgical plan $\mathbf{D}_y = \{\mathbf{d}_m^y\}_{m=1,\ldots,M}$ and intra-operative intervention $\mathbf{D}_x = \{\mathbf{d}_n^x\}_{n=1,\ldots,N}$. The normal vectors were estimated using PCA as in [15]. The proposed Bi-AGCPD method is compared against several state-of-the-art registration methods, including ICP [22], CPD [12], BCPD [13], DeepGMR [34], IGBCPD [14] and AGBCPD [15]. We have also tried other learning-based methods, which however don't perform well (similar to DeepGMR [34]) in test cases probably due to the lack of well-represented training sets.

In the first series of experiments where noise/outliers exist in $\mathbf{D}_x$(either femur or pelvis) only, the covariance matrices are $\boldsymbol{\Sigma}_{\text{Iso}} = \mathbf{I}_{3\times 3}$ and $\boldsymbol{\Sigma}_{\text{Aniso}} = \text{diag}([\frac{1}{11}, \frac{1}{11}, \frac{9}{11}])$. Different percentages of outliers are generated by displacing each point independently with a randomly generated vector whose magnitude is in the range [20,30]mm. For one specific bone model and noise type, five different percentages of outliers are tested: 10%, 30%, 50%, 70% and 90%, e.g., there are $N_{\text{outliers}} = 100 \times 10\% = 10$ outlier points in the case of 10% outliers. The evaluation metrics include the Rotational error in degree and Translation error in millimeters, which are computed as $\text{Error}_{\text{Rot}} = \arccos\left[\frac{\text{tr}\left(\mathbf{R}_{\text{true}}\mathbf{R}_{\text{cal}}^{\top}\right)-1}{2}\right] \times \frac{180^{\circ}}{\pi}$, $\text{Error}_{\text{Trans}} = \|\mathbf{t}_{\text{cal}} - \mathbf{t}_{\text{true}}\|_2$. The ground-truth rotational degree and translation vector lie in $[10, 20]^{\circ}$ and $[10, 20]$mm. In the second series of experiments where noise/outliers exist in two point sets to be registered (femur), $\boldsymbol{\Sigma}_{\text{Aniso}}$ is used and we vary the outliers percentages in $\mathbf{D}_x$ at 10%, 50%, and 90% where for each case we further vary the outliers in $\mathbf{D}_y$ at no outliers, 10%, and 30% outliers. In the third series of

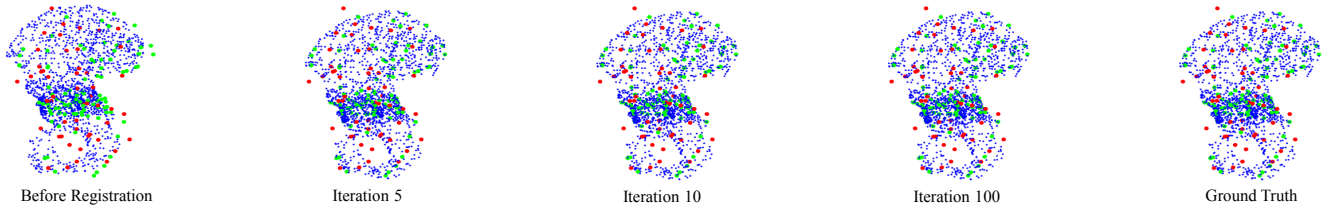

Fig. 2. Registration process using our Bi-AGCPD method with 50% outliers and anisotropic positional noise injected target point set. (a)~(d): the registration result before registration, 5th, 10th and 100th iteration using the proposed method, respectively; (e): ground truth. Blue, green, and red dots indicate the point sets $\mathbf{D}_y$, $\mathbf{D}_x$, and outliers in $\mathbf{D}_x$ respectively.

TABLE II
ROTATION AND TRANSLATION ERRORS UNDER ISOTROPIC/ANISOTROPIC NOISE TOGETHER WITH DIFFERENT PERCENTAGES OF OUTLIERS IN $\mathbf{D}_x$. FULL-TO-FULL REGISTRATION OF HUMAN PELVIS BONE.

Error Type	Outliers' Percents	10%	30%	50%	70%	90%	10%	30%	50%	70%	90%
	Noise type / Methods	Isotropic Noise					Anisotropic Noise				
Rot (°)	ICP [22]	1.0916	1.4291	1.6023	1.6663	1.9720	0.6201	1.2770	1.4827	1.7745	1.7631
	CPD [12]	2.6608	1.7717	2.6676	6.0397	4.3720	0.4557	0.2620	0.2698	0.2585	0.2557
	BCPD [13]	1.1221	1.3074	1.3672	1.5017	1.4941	1.0146	1.1445	1.2737	1.6637	1.4385
	IGBCPD [14]	0.5815	0.4925	0.4595	0.4275	0.5445	0.2413	0.4046	0.3631	0.2423	0.4428
	AGBCPD [15]	0.5501	0.5268	0.4885	0.5288	0.5278	0.1965	0.1512	0.1828	0.1911	0.1579
	Bi-IGCPD	**0.2651**	0.3060	**0.3123**	**0.3185**	**0.3219**	**0.0826**	0.0892	0.0888	**0.0875**	0.0911
	Bi-AGCPD	0.2744	**0.2815**	0.3164	0.3361	0.3460	0.1107	**0.0806**	**0.0670**	0.0907	**0.0753**
Trans (mm)	ICP [22]	0.8204	1.1200	1.2586	1.3810	1.5555	0.4528	1.0660	1.0903	1.5267	1.4029
	CPD [12]	1.4649	1.0716	1.2285	3.5516	2.2455	0.6004	0.2784	0.2633	0.3029	0.2771
	BCPD [13]	1.4606	1.2025	1.3263	1.4206	1.5672	0.9121	1.1135	1.2218	1.5032	1.5042
	IGBCPD [14]	0.5935	0.5423	0.5248	0.5815	0.5266	0.2614	0.3774	0.3439	0.2739	0.4190
	AGBCPD [15]	0.5745	0.5137	0.5116	0.5451	0.5645	0.2419	0.2591	0.2293	0.2090	0.2232
	Bi-IGCPD	0.2212	0.2490	0.2411	**0.2608**	0.2615	**0.1237**	0.1294	0.1334	0.1250	0.1460
	Bi-AGCPD	**0.2122**	**0.2269**	**0.2260**	0.2721	**0.2575**	0.1330	**0.1096**	**0.1331**	**0.1053**	**0.0972**

experiments, $\mathbf{D}_x$ (femur, with noise and outliers) covers a partial region of $\mathbf{D}_y$.

A. Noise/Outliers Exists in One Point Set

Femur Bone Table I shows mean rotational and translational error values on the femur bone point set under different percentages of outliers and two types of positional error. As it is clearly shown in Table I, the proposed method Bi-AGCPD achieves the lowest rotational and translational error values at all percentages of outliers. It is also noteworthy that the simplified variant Bi-IGCPD (isotropic positional noise) outperforms IGBCPD [14] and AGBCPD [15], which demonstrates the significance of incorporating the bi-directional mechanism. In addition, both registration error values of Bi-IGCPD and Bi-AGCPD are quite stable with increasing percentages of outliers which is partly attributed to the utilisation of normal vectors. DeepGMR fails in all cases with registration errors being $> 30°$ and > 10mm.

Pelvis Bone Table II shows results on the pelvis point set. As shown in Table II, the best performances are achieved with either proposed Bi-IGCPD or Bi-AGCPD methods, which validates the effectiveness of the bi-directional mechanism and additional normal vectors. DeepGMR [34] still performs poorly like in Table I, thus we don't add its results in Table II. Fig. 2 shows the registration performance with the iterations. As shown in Fig. 2, Bi-AGCPD converges quickly almost after 10 EM iterations by noticing the small(even negligible) difference between registration error values after 10 iterations ($0.0823°$ and 0.0356mm) and 100 iterations ($0.0819°$ and 0.0252mm).

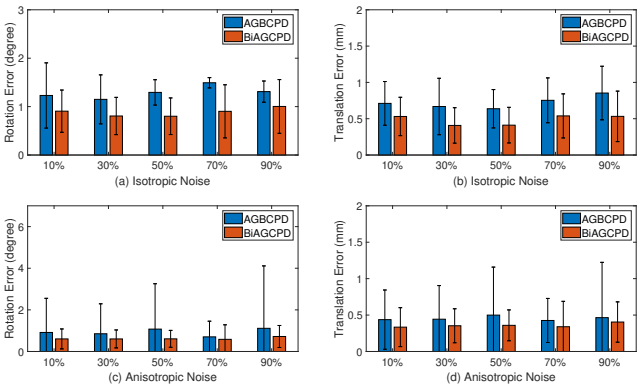

Fig. 3. Mean and standard deviation of rotation and translation error using AGBCPD [15] and Bi-AGCPD under different percentages of outliers. (a) and (b): isotropic positional noise; (c) and (d): anisotropic positional noise.

B. Noise/Outliers Exists in Two Point Sets

Table III includes the mean rotational and translational error values when noise and outliers exist in both $\mathbf{D}_x$ and $\mathbf{D}_y$. Similarly, DeepGMR exceeds $40°$ and 15 mm

TABLE III
ROTATION AND TRANSLATION ERRORS UNDER ANISOTROPIC NOISE TOGETHER WITH DIFFERENT PERCENTAGES OF OUTLIERS IN $\mathbf{D}_x$ AND $\mathbf{D}_y$. FULL-TO-FULL REGISTRATION OF HUMAN FEMUR BONE.

Error Type	Outliers' Percents in X	10%	50%	90%	10%	50%	90%	10%	50%	90%
	Methods	no outliers in Y			10% outliers in Y			30% outliers in Y		
Rot (°)	ICP [22]	2.4140	4.8358	5.0818	3.5212	7.5922	7.8942	9.3679	9.3826	9.5348
	CPD [12]	0.6172	0.7536	3.7813	0.6588	1.5288	0.9803	0.7791	0.9405	1.2408
	BCPD [13]	1.2070	2.7412	5.6808	1.3257	2.2989	4.3093	1.3332	2.1632	4.1456
	IGBCPD [14]	0.4669	0.4526	0.6836	0.5991	0.6273	0.6933	0.5898	0.5791	0.5903
	AGBCPD [15]	0.4072	0.4368	0.5342	0.3928	0.4429	0.6094	0.4415	0.3854	0.5545
	Bi-IGCPD	0.2183	0.2391	0.3019	0.2233	0.2283	0.2681	0.2235	0.2308	0.2301
	Bi-AGCPD	**0.1753**	**0.1758**	**0.2002**	**0.1771**	**0.1857**	**0.1959**	**0.1749**	**0.1884**	**0.1791**
Trans (mm)	ICP [22]	1.0911	1.9122	2.0686	1.3120	2.7646	2.8250	5.4276	4.3519	4.0436
	CPD [12]	0.4250	0.4544	1.2187	0.4375	0.7082	0.6431	0.4644	0.5332	0.8816
	BCPD [13]	0.4908	1.1508	2.2434	0.4895	0.9210	1.8709	0.5240	0.9638	1.6255
	IGBCPD [14]	0.4066	0.4124	0.4746	0.4363	0.4162	0.4736	0.4112	0.4139	0.4390
	AGBCPD [15]	0.4296	0.3730	0.5398	0.4317	0.4344	0.4249	0.3681	0.4397	0.4402
	Bi-IGCPD	0.2313	0.2102	0.2978	0.2326	0.2338	0.2985	0.2216	0.2130	0.2409
	Bi-AGCPD	**0.1639**	**0.1549**	**0.1701**	**0.1725**	**0.1651**	**0.1754**	**0.1853**	**0.1748**	**0.1778**

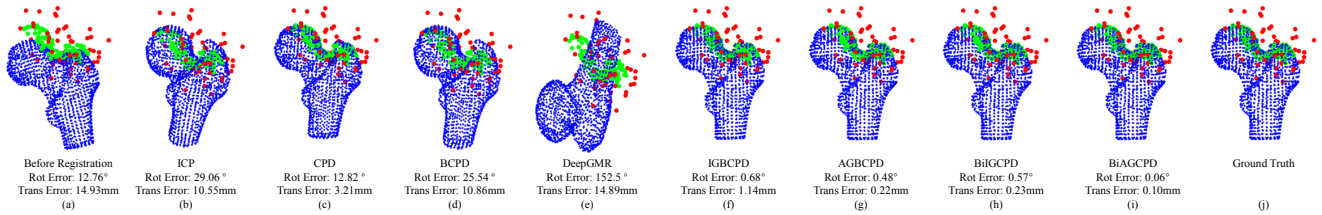

Fig. 4. Subfigure (a) shows two point sets before registration where anisotropic noise and 50% outliers exist in $\mathbf{D}_x$. Subfigures (b)~(i) show registration results using ICP [22], CPD [12], BCPD [13], DeepGMR [34], IGBCPD [14], AGBCPD [15], our Bi-IGCPD and Bi-AGCPD respectively. Subfigure (j) shows two point sets after registration with ground-truth transformation. Blue, green, and red dots are point sets $\mathbf{D}_y$, $\mathbf{D}_x$, and outliers in $\mathbf{D}_x$ respectively.

respectively in almost all cases of this experiments series, thus its results are not reported. Both Bi-IGCPD and Bi-AGCPD outperform the previous methods and their results are not susceptible to increasing outliers. The bidirectional mechanism improves the robustness and accuracy of the registration.

C. Partial-to-full Registration

Fig. 3 shows the rotational and translation error values under noise and outliers, for aligning the intra-operative partial femur points with the pre-operative full model. As can be seen from Fig. 3, the bi-directional mechanism can further enhance the registration performance by observing the smaller error values compared to AGBCPD. Fig. 4 shows the qualitative results of all compared methods, which shows that the position-only-based registration methods (i.e., ICP, CPD, BCPD) and DeepGMR ($152.5°$ and 14.89mm) fail to align the two point sets with $> 12°$ and > 3mm. Bi-AGCPD achieves lower rotational and translational error values than all compared.

D. The Impact of Bidirectional Weight α

Fig. 5 shows the rotational and translational error values of full-to-full registration for femur bone, with varying weight α of forward posterior probability in four cases. As it can be seen in Fig. 5, most registration error values are the largest at $\alpha = 1$, and are smaller at other values of α, which reflects the significance of utilising the bi-directional mechanism. It

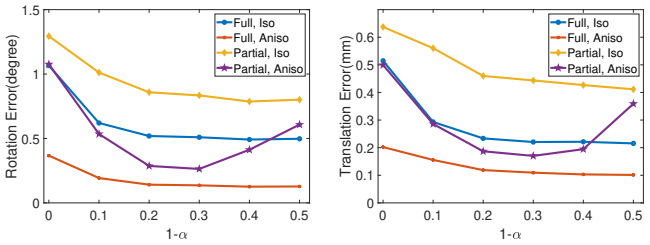

Fig. 5. Rotational (left) and translational (right) error values of BiAGCPD on the femur with varying α for four cases: (1) full-to-full registration, isotropic noise; (2) full-to-full registration, anisotropic noise; (3) partial-to-full registration, isotropic noise; (4) partial-to-full with anisotropic noise.

is noted that AGBCPD can be as a special case of Bi-AGCPD where $\alpha = 1$. For different data types and noise types, the optimal α is different. As can be seen from Fig. 5, even if the weight of backward posterior (1-α) is small, it can still bring a big improvement w.r.t. AGBCPD ($\alpha = 1$).

VI. CONCLUSIONS

This paper proposes novel bidirectional generalised coherent point drift methods to solve the generalised rigid point set registration problem, under isotropic and anisotropic positional uncertainties. Experiments on different human bones validate the improvements of the proposed method over existing probabilistic and learning-based methods, which also demonstrates great potential for image-guided surgery.

REFERENCES

[1] R. H. Taylor, N. Simaan, A. Menciassi, and G.-Z. Yang, "Surgical robotics and computer-integrated interventional medicine," *Proceedings of the IEEE*, vol. 110, no. 7, pp. 823–834, 2022.

[2] Z. Yaniv, "Registration for orthopaedic interventions," in *Computational radiology for orthopaedic interventions*. Springer, 2016, pp. 41–70.

[3] B. Maiseli, Y. Gu, and H. Gao, "Recent developments and trends in point set registration methods," *Journal of Visual Communication and Image Representation*, vol. 46, pp. 95–106, 2017.

[4] X. Huang, G. Mei, J. Zhang, and R. Abbas, "A comprehensive survey on point cloud registration," *arXiv preprint arXiv:2103.02690*, 2021.

[5] A. Fan, J. Ma, X. Tian, X. Mei, and W. Liu, "Coherent point drift revisited for non-rigid shape matching and registration," in *Proceedings of the IEEE/CVF Conference on Computer Vision and Pattern Recognition*, 2022, pp. 1424–1434.

[6] A. Fan, J. Ma, X. Jiang, and H. Ling, "Efficient deterministic search with robust loss functions for geometric model fitting," *IEEE Transactions on Pattern Analysis and Machine Intelligence*, pp. 1–1, 2021.

[7] A. Fan, X. Jiang, Y. Ma, X. Mei, and J. Ma, "Smoothness-driven consensus based on compact representation for robust feature matching," *IEEE Transactions on Neural Networks and Learning Systems*, 2021.

[8] J. Ma, Y. Ma, and C. Li, "Infrared and visible image fusion methods and applications: A survey," *Information Fusion*, vol. 45, pp. 153–178, 2019.

[9] J. Ma, X. Jiang, A. Fan, J. Jiang, and J. Yan, "Image matching from handcrafted to deep features: A survey," *International Journal of Computer Vision*, vol. 129, no. 1, pp. 23–79, 2021.

[10] Z. Deng, Y. Yao, B. Deng, and J. Zhang, "A robust loss for point cloud registration," in *Proceedings of the IEEE/CVF International Conference on Computer Vision*, 2021, pp. 6138–6147.

[11] J. Ma, A. Fan, X. Jiang, and G. Xiao, "Feature matching via motion-consistency driven probabilistic graphical model," *International Journal of Computer Vision*, vol. 130, no. 9, pp. 2249–2264, 2022.

[12] A. Myronenko and X. Song, "Point set registration: Coherent point drift," *IEEE transactions on pattern analysis and machine intelligence*, vol. 32, no. 12, pp. 2262–2275, 2010.

[13] O. Hirose, "A bayesian formulation of coherent point drift (vol 43, pg 2269, 2021)," *IEEE transactions on pattern analysis and machine intelligence*, vol. 43, no. 9, pp. 3273–3273, 2021.

[14] A. Zhang, Z. Min, J. Pan, and M. Q.-H. Meng, "Robust and accurate point set registration with generalized bayesian coherent point drift," in *2021 IEEE/RSJ International Conference on Intelligent Robots and Systems (IROS)*. IEEE, 2021, pp. 516–523.

[15] A. Zhang, Z. Min, X. Yang, Z. Zhang, J. Pan, and M. Q.-H. Meng, "Generalized 3d rigid point set registration with anisotropic positional error based on bayesian coherent point drift," in *2022 International Conference on Robotics and Automation (ICRA)*. IEEE, 2022, pp. 3790–3796.

[16] J. Luo, A. Sedghi, K. Popuri, D. Cobzas, M. Zhang, F. Preiswerk, M. Toews, A. Golby, M. Sugiyama, W. M. Wells *et al.*, "On the applicability of registration uncertainty," in *International Conference on Medical Image Computing and Computer-Assisted Intervention*. Springer, 2019, pp. 410–419.

[17] J. Luo, S. Frisken, D. Wang, A. Golby, M. Sugiyama, and W. Wells III, "Are registration uncertainty and error monotonically associated?" in *International Conference on Medical Image Computing and Computer-Assisted Intervention*. Springer, 2020, pp. 264–274.

[18] S. Herregodts, M. Verhaeghe, B. De Coninck, M. Forward, M. A. Verstraete, J. Victor, and P. De Baets, "An improved method for assessing the technical accuracy of optical tracking systems for orthopaedic surgical navigation," *The International Journal of Medical Robotics and Computer Assisted Surgery*, vol. 17, no. 4, p. e2285, 2021.

[19] Z. Min, H. Ren, and M. Q.-H. Meng, "Statistical model of total target registration error in image-guided surgery," *IEEE Transactions on Automation Science and Engineering*, vol. 17, no. 1, pp. 151–165, 2019.

[20] Z. Min and M. Q.-H. Meng, "General first-order target registration error model considering a coordinate reference frame in an image-guided surgical system," *Medical & Biological Engineering & Computing*, vol. 58, no. 12, pp. 2989–3002, 2020.

[21] H. Yang, J. Shi, and L. Carlone, "Teaser: Fast and certifiable point cloud registration," *IEEE Transactions on Robotics*, 2020.

[22] P. J. Besl and N. D. McKay, "Method for registration of 3-d shapes," in *Sensor fusion IV: control paradigms and data structures*, vol. 1611. International Society for Optics and Photonics, 1992, pp. 586–606.

[23] J. Yang, H. Li, D. Campbell, and Y. Jia, "Go-icp: A globally optimal solution to 3d icp point-set registration," *IEEE transactions on pattern analysis and machine intelligence*, vol. 38, no. 11, pp. 2241–2254, 2015.

[24] J. Hermans, D. Smeets, D. Vandermeulen, and P. Suetens, "Robust point set registration using em-icp with information-theoretically optimal outlier handling," in *CVPR 2011*. IEEE, 2011, pp. 2465–2472.

[25] S. Billings and R. Taylor, "Iterative most likely oriented point registration," in *International Conference on Medical Image Computing and Computer-Assisted Intervention*. Springer, 2014, pp. 178–185.

[26] L. Li, M. Yang, C. Wang, and B. Wang, "Robust point set registration using signature quadratic form distance," *IEEE transactions on cybernetics*, vol. 50, no. 5, pp. 2097–2109, 2018.

[27] B. Jian and B. C. Vemuri, "Robust point set registration using gaussian mixture models," *IEEE transactions on pattern analysis and machine intelligence*, vol. 33, no. 8, pp. 1633–1645, 2010.

[28] G. D. Evangelidis and R. Horaud, "Joint alignment of multiple point sets with batch and incremental expectation-maximization," *IEEE transactions on pattern analysis and machine intelligence*, vol. 40, no. 6, pp. 1397–1410, 2017.

[29] Y. Wang and J. M. Solomon, "Deep closest point: Learning representations for point cloud registration," in *Proceedings of the IEEE/CVF international conference on computer vision*, 2019, pp. 3523–3532.

[30] Z. J. Yew and G. H. Lee, "Rpm-net: Robust point matching using learned features," in *Proceedings of the IEEE/CVF conference on computer vision and pattern recognition*, 2020, pp. 11 824–11 833.

[31] Y. Aoki, H. Goforth, R. A. Srivatsan, and S. Lucey, "Pointnetlk: Robust & efficient point cloud registration using pointnet," in *Proceedings of the IEEE/CVF Conference on Computer Vision and Pattern Recognition*, 2019, pp. 7163–7172.

[32] X. Li, J. K. Pontes, and S. Lucey, "Pointnetlk revisited," in *Proceedings of the IEEE/CVF Conference on Computer Vision and Pattern Recognition (CVPR)*, June 2021, pp. 12 763–12 772.

[33] S. Huang, Z. Gojcic, M. Usvyatsov, A. Wieser, and K. Schindler, "Predator: Registration of 3d point clouds with low overlap," in *Proceedings of the IEEE/CVF Conference on computer vision and pattern recognition*, 2021, pp. 4267–4276.

[34] W. Yuan, B. Eckart, K. Kim, V. Jampani, D. Fox, and J. Kautz, "Deepgmr: Learning latent gaussian mixture models for registration," in *European conference on computer vision*. Springer, 2020, pp. 733–750.

[35] C. Choy, W. Dong, and V. Koltun, "Deep global registration," in *Proceedings of the IEEE/CVF conference on computer vision and pattern recognition*, 2020, pp. 2514–2523.

[36] X. Huang, G. Mei, and J. Zhang, "Feature-metric registration: A fast semi-supervised approach for robust point cloud registration without correspondences," in *Proceedings of the IEEE/CVF conference on computer vision and pattern recognition*, 2020, pp. 11 366–11 374.

[37] C. Raposo and J. P. Barreto, "Using 2 point+ normal sets for fast registration of point clouds with small overlap," in *2017 IEEE International Conference on Robotics and Automation (ICRA)*. IEEE, 2017, pp. 5652–5658.

[38] K. Jordan and P. Mordohai, "A quantitative evaluation of surface normal estimation in point clouds," in *2014 IEEE/RSJ International Conference on Intelligent Robots and Systems*. IEEE, 2014, pp. 4220–4226.

[39] S. Billings and R. Taylor, "Generalized iterative most likely oriented-point (g-imlop) registration," *International journal of computer assisted radiology and surgery*, vol. 10, no. 8, pp. 1213–1226, 2015.

[40] W. Liu, H. Wu, and G. S. Chirikjian, "Lsg-cpd: Coherent point drift with local surface geometry for point cloud registration," in *Proceedings of the IEEE/CVF International Conference on Computer Vision*, 2021, pp. 15 293–15 302.

[41] Z. Min, D. Zhu, J. Liu, H. Ren, and M. Q.-H. Meng, "Aligning 3d curve with surface using tangent and normal vectors for computer-assisted orthopedic surgery," *IEEE Transactions on Medical Robotics and Bionics*, vol. 3, no. 2, pp. 372–383, 2021.